Two-Phase Flow in Smooth and Rough Fractures: Measurement and Correlation by Porous-Medium and Pipe Flow Models

M. Fourar and S. Bories

Institut de Mécanique des Fluides de Toulouse, Toulouse, France

R. Lenormand

Institut Français du Pétrole, Rueil Malmaison, France

P. Persoff

Earth Sciences Division, Lawrence Berkeley Laboratory, Berkeley, California

Two-phase (air-water) flow experiments were conducted in horizontal artificial fractures. The fractures were between glass plates that were either smooth or artificially roughened by gluing a layer of glass beads to them. One smooth fracture with an aperture of 1 mm and three rough fractures, one with the two surfaces in contact and two without contact, were studied. For both types of fractures, the flow structures are similar to those observed in two-phase flow in a pipe, with structures (bubbles, fingering bubbles, films, and drops) depending on the gas and liquid flow rates. The pressure gradients measured for different liquid and gas velocities were interpreted by three models. First, using Darcy's law leads to relative permeability curves similar to conventional ones for porous media. However, these curves depend not only on saturation but also on flow rates. This effect is caused by inertial forces which are not included in this approach. Second, the standard approach for two-phase flow in pipes (Lockhart and Martinelli's equation) agrees with experimental results, at least for small pressure gradients. Finally, the best fit was obtained by treating the two phases as one homogeneous phase. All the properties are averaged, and the pressure drop is deduced from an empirical correlation between the two-phase Reynolds number and the friction factor.

Introduction

Two-phase flow in fractured rocks occurs in several important applications: in oil or gas recovery, in exploitation of geothermal energy, in the storage of radioactive waste, etc. Models to predict two-phase flow in fractures are therefore of practical interest, although little is known of the laws governing such flows. In the subsurface environment, the fluids generally flow through a network of intersecting fractures. The study of two-phase flow in a single fracture is basic to understanding flow in complex networks of fractures.

Fracture flow can be considered either as a limiting case of flow in a porous medium or as a limiting case of pipe flow. Historically, the porous-medium approach has been used for situations involving subsurface flow. This approach emphasizes the importance of capillary and viscous forces, with negligible inertial forces. Under conditions of high velocity and relatively open fractures such as those intersecting a production well, the mechanisms may approach the limiting case of two-phase pipe flow.

In the porous-medium approach, Darcy's law is written for each phase. For horizontal flow (no gravity effect):

$$V_{LS} = - \frac{k_0 Kr_L}{\mu_L} \frac{dP_L}{dx} \tag{1}$$

$$V_{GS} = - \frac{k_0 Kr_G}{\mu_G} \frac{dP_G}{dx} \tag{2}$$

where subscripts L and G stand for liquid and gas, respectively; V_{LS} and V_{GS} are superficial velocities equal to the flow rate per unit cross-section area of the sample; P is the pressure; μ is the viscosity; k_0 is the intrinsic (single-phase) permeability; and Kr is the relative permeability.

The relative permeability accounts for the fact that each phase interferes with the flow of the other, and (at least in porous media) Kr_L and Kr_G are highly dependent upon phase saturation. Owing to lack of data, it is generally assumed that in fractures, the relative permeability to each phase is equal to its saturation, i.e. that neither phase interferes with the flow of the other. Consequently, $Kr_L + Kr_G = 1$. This assumption is based on experimental work by *Romm* [1966], in which oil and water were confined in different stripes of a smooth fracture by controlling the wettability of the surfaces and also on analysis of field data from geothermal reservoirs [*Pruess et al.*, 1983, 1984; *Mendoza and Sudicky*, 1991]. On the other hand, theoretical analysis and numerical simulations by *Pruess and Tsang* [1990] and *Pyrak-Nolte et al.* [1992] showed that significant phase interference would occur in a rough fracture. This was confirmed by experimental work [*Persoff et al.*, 1991; *Fourar et al.*, 1991, *Fourar*, 1992].

In this paper we present additional results concerning the pressure drops during liquid/gas flow in smooth and rough fractures and their interpretation by using three models available in the literature. The experimental setup is de-
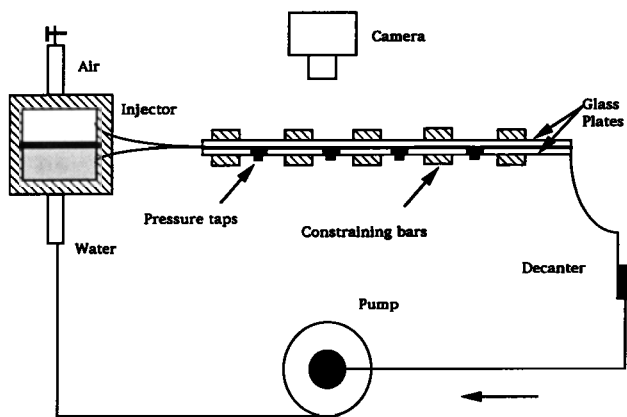
Fig. 1. Experimental equipment.

scribed in the first part of this paper. Then the results concerning the flow structures and the pressure gradients are presented. The data are subsequently analyzed using three different models: (1) relative permeabilities (porous-medium approach), (2) Lockhart and Martinelli's model (pipe flow approach), and (3) homogeneous model. The two first models consider separate equations for the two fluids. The main difference is the role of inertial forces, which are neglected in the first model. On the other hand, the third model uses the standard approach of pressure drop in a rough tube for a single-phase turbulent flow, through the notion of friction factor. The artificial single-phase fluid is defined by averaging all the properties of the two fluids.

EXPERIMENTAL SETUP

The principle of the experimental setup is shown in Figure 1. The fracture consisted of two horizontal glass plates 1 m long and 0.5 m wide. The plates were either smooth or artificially roughened. One set of experiments (S) was performed with the smooth plates. Three sets of experiments were performed with the rough plates: one with the rough surfaces in contact (R1) and two with the surfaces spaced apart (R2 and R3). The smooth fracture was assembled by placing 1-mm-thick strips of stainless steel along the no-flow boundaries. Rough surfaces were made by applying a 0.3-mm-thick layer of transparent epoxy cement to the surfaces and gluing a single layer of 1-mm-diameter glass beads to each plate. Figure 2 shows a sample of the roughness pattern. For experiment R1, the two surfaces were placed in contact and silicone caulk was used to seal the no-flow boundaries. Two additional experiments, R2 and R3, were done by disassembling R1 and reassembling it with 3-mm-thick stainless steel strips and caulk along the no-flow boundaries. Therefore R2 had an approximately 1-mm clearance between the rough surfaces. R3 was prepared by disassembling R2, reassembling it with more silicone caulk along the no-flow boundaries, and increasing the clearance between the rough surfaces slightly (by about 0.1 mm). Steel bars were tightened in place to prevent the glass from bulging at high flow rates for all fractures.

The injector consisted of 500 stainless steel tubes of 1-mm outside diameter and 0.66-mm inside diameter. Air and water were injected through alternating tubes to achieve uniform distribution of flow at the inlet. Air was injected at constant pressure, and its volume flow rate was measured by an in-line rotameter and corrected to standard pressure.
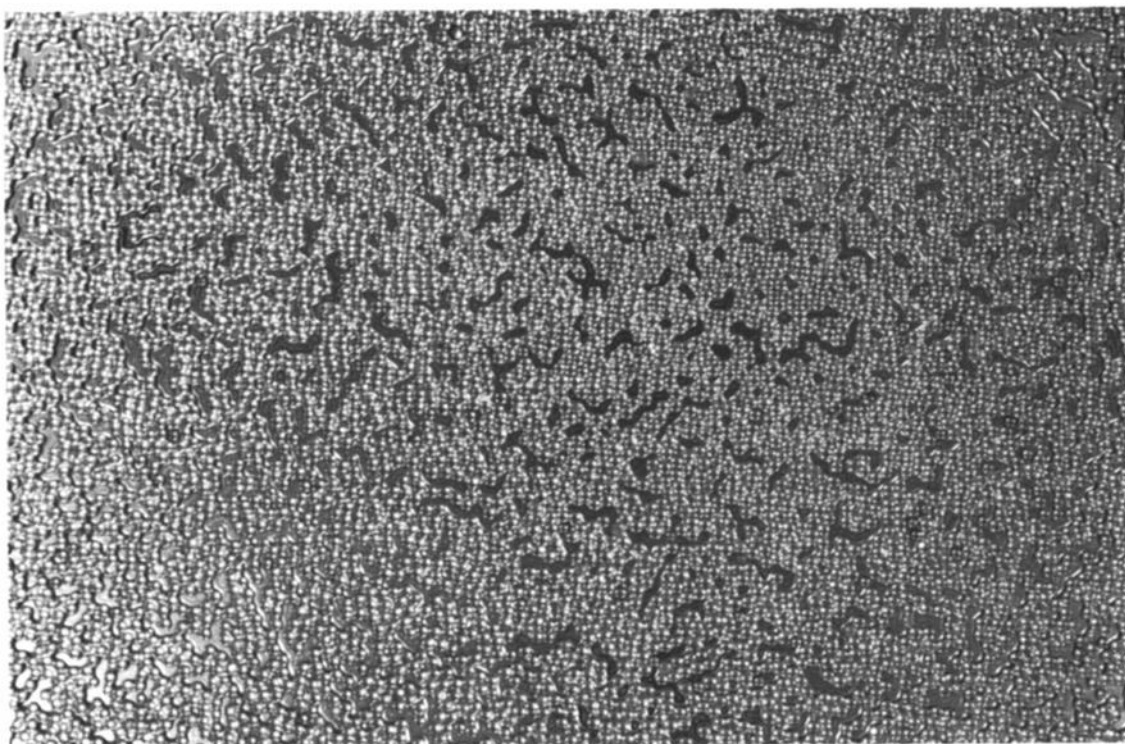

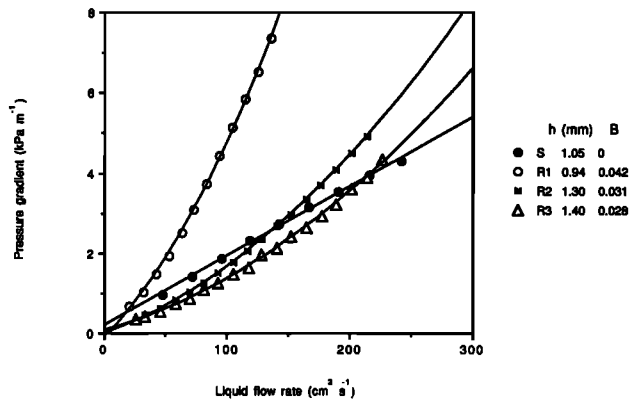Fig. 2. Photograph of the rough surface used in the experiments (bead diameter equals 1 mm).

Fig. 3. Pressure drop in single-phase liquid flow plotted against flow rate. Parabolic curves for the rough-walled fractures indicate deviation from Darcy's law. Values of h and B are obtained by root-mean-square fit (4).

Water was injected by a calibrated pump. At the outlet of the fracture, gas escaped to the atmosphere and water was collected in a decanter and recycled.

Liquid saturation was measured by a volume balance method. The water volume in the decanter was measured at the beginning of the experiment with the fracture completely saturated with flowing water and again when steady state had been reached at each airflow rate. Changes in the water volume in the decanter were then used to calculate the liquid saturation in the fracture. A good agreement was found between this method and the saturation measurements obtained by the surface ratio of the fluids on the photographs. The volume balance method was used to measure liquid saturation in the rough fractures, which could not be estimated from photographs.

Nine liquid-filled pressure taps were cemented into holes drilled along the centerline of the lower plate. Any pair of taps could be connected by valves to a differential transducer. Since the pressure gradient fluctuates rapidly, only the time-averaged values were recorded.

The fracture was initially saturated with water. Water was injected at a constant rate through the fracture before each experiment. Air injection was then started and increased stepwise. When steady state was reached for each flow rate, the pressure gradient and liquid saturation were measured. Then the fracture was resaturated with water, and the experiment was repeated several times at different liquid flow rates. Videotape and photography were used to record the distribution and motion of phases through the fracture.

EXPERIMENTAL RESULTS

Calculation of Hydraulic Aperture

The hydraulic aperture h of each fracture was calculated from a single-phase flow experiment. Laminar flow through a fracture with smooth parallel sides obeys Darcy's law with single-phase permeability k_0 [Witherspoon et al., 1980]:

$$k_0 = h^2/12 \qquad (3)$$

The pressure drop for the gas flow was too small to be measured reliably. Pressure drop in single-phase liquid flow for the four fractures is shown in Figure 3. The smooth-

fracture data plot as a straight line, while the rough-fracture data plot as parabolas. Deviation from linearity for rough fractures indicates deviation from Darcy's law but does not necessarily indicate turbulent flow. Such deviation has been observed in porous media (see reviews by Houpeurt [1974] and Temeng and Horne [1988]) and in rough fractures [Schrauf and Evans, 1986]. The deviation from Darcy's law is caused by inertial forces, which are proportional to the square of the filtration velocity V_{LS} and the density ρ. The relationship between pressure gradient and flow rate is then written

$$-\frac{dP}{dx} = \frac{12\mu}{h^3} Q + B \frac{\rho}{h^3} Q^2 \qquad (4)$$

Q is the volumetric flow rate per unit width, and B is a dimensionless number function of the roughness of the walls. Values of h and B determined from the parabolas are shown in Figure 3. For the smooth fracture the value $h = 1.05$ mm agrees with the real spacing of 1 mm between the plates. For the rough fractures the values are also in agreement with an estimate of the mean spacing between the plates.

Hydraulic apertures found in the field are generally smaller than those in our experimental fractures. Romm [1966] states that most fractures are in the range of 0.015 to 0.04 mm. However, Raven et al. [1988] inferred fracture hydraulic apertures from pumping tests and found many sizes to be in the 0.1- to 0.2-mm range.

Flow Structures

In two-phase flow, essentially the same range of flow structures was observed in both smooth and rough fractures with and without contact, as shown in Figure 4. These flow structures were constantly in motion, never stopping even momentarily.

The flow structures varied over the range of liquid and gas flow rates studied as shown in Figures 5a and 5b. For the smooth fracture (Figure 5a) the different flow patterns can be observed at a constant liquid velocity (for instance, around 0.1 m s^{-1}). At low gas flow rate, we observe gas bubbles dispersed in the flowing liquid. Increasing the gas flow rate increases the size of the bubbles, which start to become unstable by tip-splitting (fingering bubbles). For a gas velocity larger than 0.3 m s^{-1}, the flow becomes chaotic with no apparent structures. At higher gas velocity, the gas occupies the main part of the fracture, the liquid flowing as unstable films along the walls. However, for low liquid velocities, the films are replaced by liquid drops dispersed in the flowing gas. The structures are similar for the rough fracture (Figure 5b).

The aforementioned flow structures show more similarity to the structures observed in pipe flow than to the structures expected for a porous medium. In a porous medium it is generally assumed (but not experimentally verified) that in Darcy's regime, the wetting phase occupies the smallest pores and the nonwetting phase occupies the largest pores. Accordingly, for any fixed value of saturation, each phase occupies its own network of pores, and each network is continuous from inlet to outlet. The phase occupancy of the pore space, which determines the relative permeability, is solely a function of the saturation. Fluids flow through these

SMOOTH   ROUGH

bubbles

**fingering
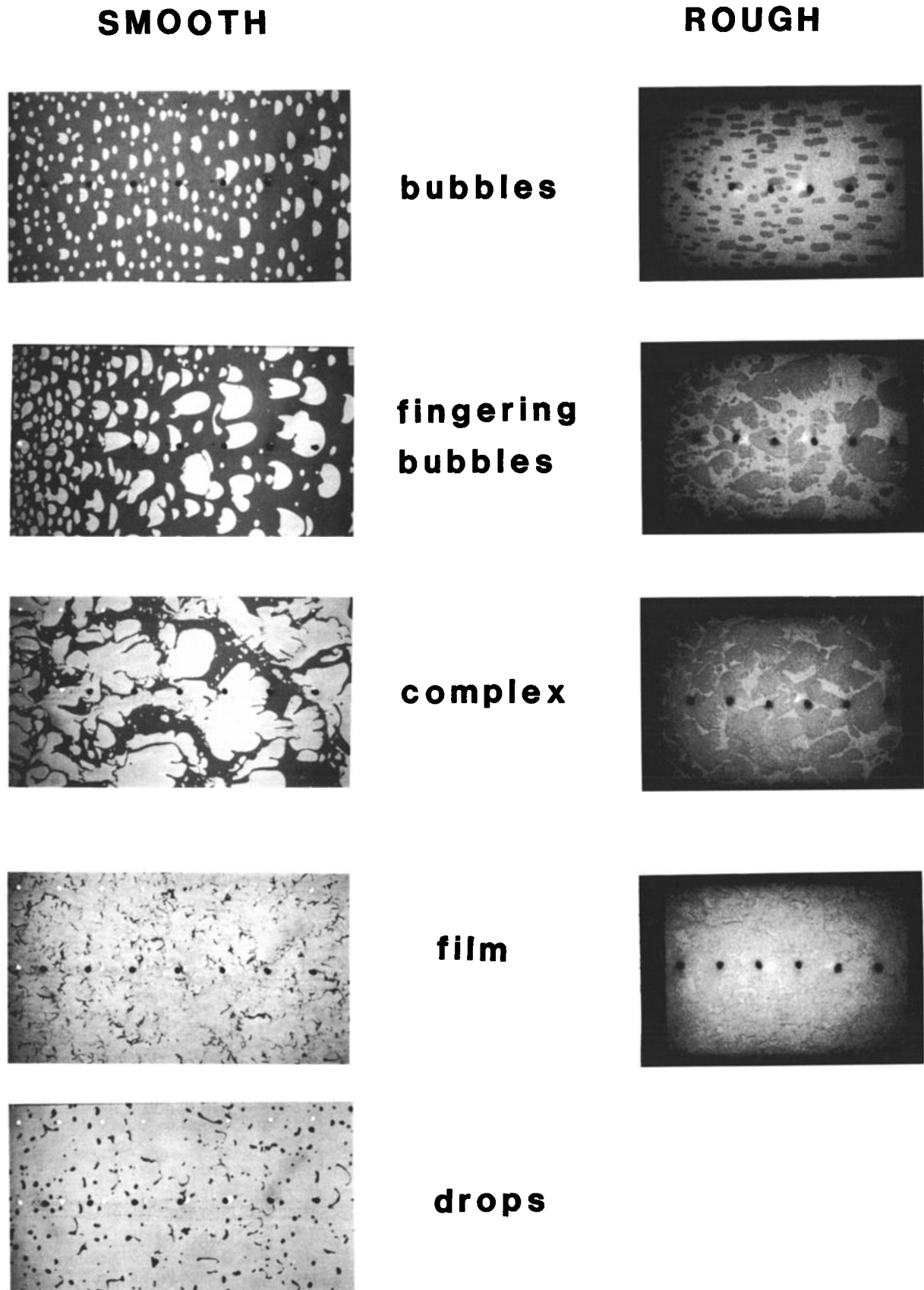bubbles**

complex

film

drops

Fig. 4.   The five flow structures were observed in both smooth and rough fractures. Here, flow is from left to right. The liquid contained dye and appears dark in the smooth fracture, while the liquid contained no dye and appears light in the rough fractures.
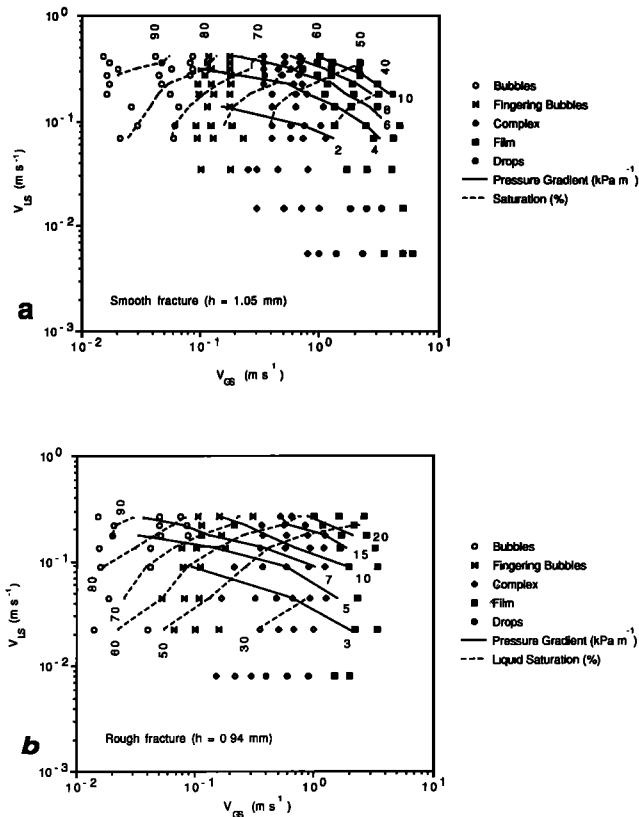
Fig. 5. Flow structure maps with contours of pressure gradient and liquid saturation: (a) smooth fracture; (b) rough fracture R1 with contact.

fixed networks when the steady state is reached. However, when the flow rate is varied, these networks can change during a transient regime. In our experiments we see quite the opposite. Only one phase is continuous, with the other phase flowing as discrete drops or bubbles except perhaps in the chaotic-flow region. In general, no spot in the fracture is ever occupied continuously by either phase. The flow structures are essentially similar whether the glass plates are smooth, rough with contact, or rough without contact.

The formation of moving flow structures, rather than stable flow paths, appears to result from the nature of the artificial roughness and the velocities used in the experiments, both of which tend to make inertial forces large compared to capillary forces. In any rough fracture, natural or artificial, the aperture varies from point to point. Regions of small aperture attract the wetting phase, and regions of large aperture attract the nonwetting phase. If these regions are large enough, they tend to form flow paths for the respective phases. In our artificial fractures, these regions are much smaller than in real fractures. To this end, consider that in our artificial rough fractures the aperture varies from its local minimum (near zero for R1, near 1 mm for R2 and R3) to its maximum (approximately 2 mm greater than the minimum) over a horizontal distance of one bead diameter (1 mm). By contrast, in a natural fracture the aperture varies much more gradually (see, for example, the data sets of *Cox and Wang* [1993] or the correlation deduced from power spectra on real fractures obtained by *Brown and Kraus* [1986]). If the natural fracture is discretized into 1-cm² squares, some squares will be more attractive to the wetting

phase and others will be more attractive to the nonwetting phase, but if the artificial fracture is discretized, then because of an averaging effect, all the squares will be equally attractive to either phase. Under these conditions the capillary forces, which tend to hold the phases in stable paths, are outweighed by the inertial forces, which tend to cause the structure to move. As flow velocities decrease, capillary forces become relatively more important and inertial forces become less important; however, capillary forces are never dominant in any part of Figure 5.

Two-Phase Pressure Drop

The first observation is that the pressure difference is the same between any pair of adjacent transducers. Consequently, we can use only one pressure gradient for an experiment. The pressure gradients and liquid saturations are plotted as smooth contours in Figures 5a and 5b. We note that there is no sharp variation in the pressure gradient when the flow structure changes, unlike flow in pipes. That suggests that the same model may be adequate to describe flow in all regions from bubbles to film.

INTERPRETATION

Correlation of flow rates, pressure drop, and saturation is a major goal of this study. We have examined three models: (1) porous medium, (2) pipe flow, and (3) equivalent homogeneous flow.

Generalized Darcy Model

Since the generalized Darcy model is based on viscous pressure drop, we expect only poor agreement. However, this model is generally used in the petroleum industry for a fractured reservoir, and it is useful to test it on these experiments.

We suppose that the two-phase flow in a fracture is governed by the generalized Darcy law (1) and (2). In these equations, relative permeability expresses the degree to which each phase impedes the flow of the other. The capillary pressure ($P_C = P_G - P_L$) is negligible in our experiment. Then, $dP/dx = dP_L/dx = dP_G/dx$, where dP/dx is the observed pressure gradient under two-phase flow conditions. Substituting (3) into (1) and (2) leads to the relative permeabilities,

$$Kr_L = -\frac{12\mu_L V_L}{h^2 \dfrac{dP}{dx}} \tag{5}$$

$$Kr_G = -\frac{12\mu_G V_G}{h^2 \dfrac{dP}{dx}} \tag{6}$$

The calculated Kr_L and Kr_G are plotted as a function of the measured saturation in Figures 6a and 6b. In these figures (and the figures that follow), the different symbols represent individual experiments in which the liquid velocity V_{LS} is held constant and the gas velocity V_{GS} is increased. These curves are qualitatively similar to conventional curves obtained in porous media. However, a family of curves depending on V_{LS} is found instead of the single curve found in porous media. Relative permeabilities are therefore not
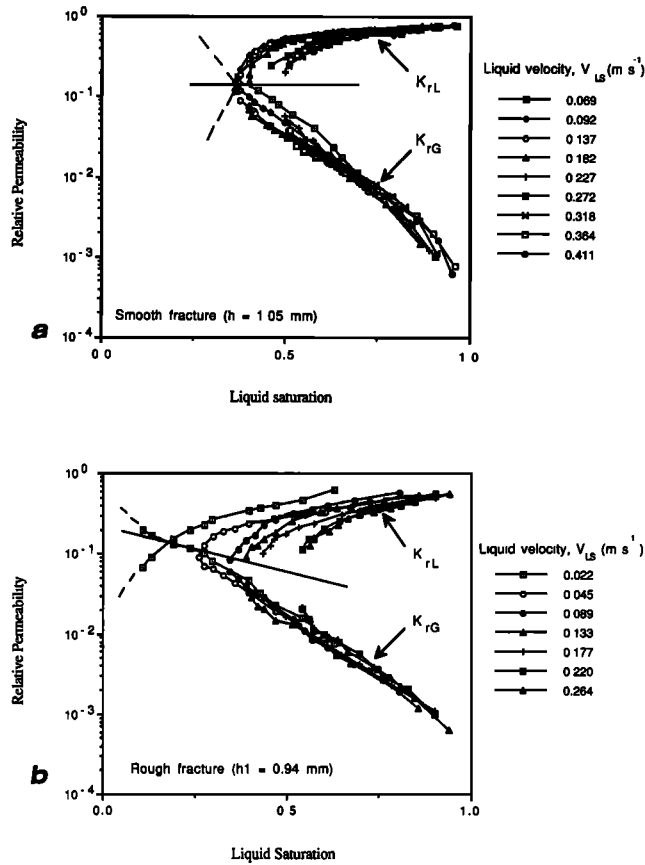
Fig. 6. Generalized Darcy model: relative permeability as a function of liquid saturation: (a) smooth fracture; (b) rough fracture.
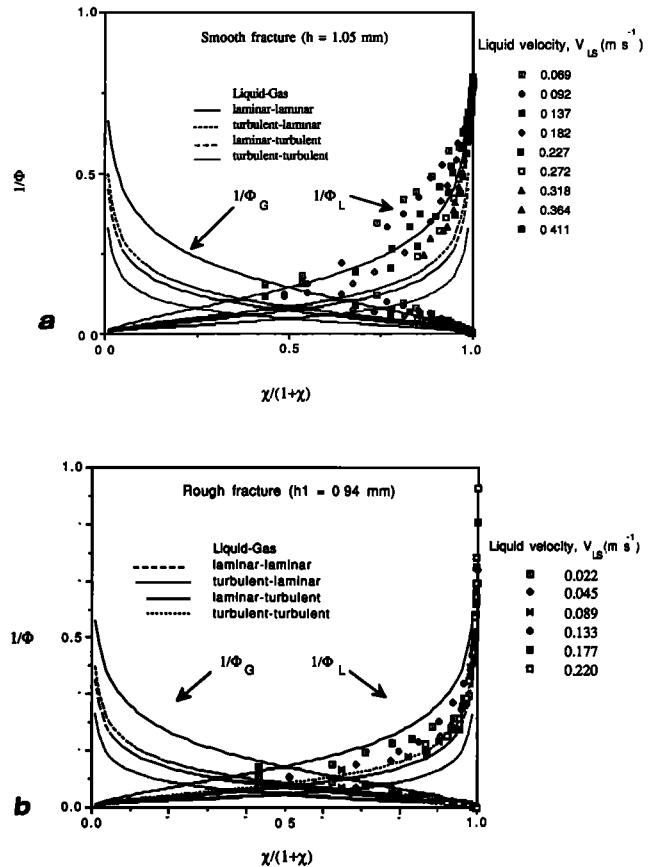

Fig. 7. Lockhart and Martinelli's model: relationship between $1/\Phi$ and $\chi/(1 + \chi)$: (a) smooth fracture; (b) rough fracture.

solely functions of saturation under these conditions, and the sum of Kr_L and Kr_G is less than 1 at all saturations. Thus significant phase interference occurs even in the smooth fracture, and relative permeabilities are not linearly dependent on saturation as is commonly assumed for reservoir simulations.

Lockhart and Martinelli's Model

The similarity of flow structures to those observed in pipe suggests the use of a model developed for two-phase flow in pipes (the Lockhart and Martinelli [1949] model; see also Perry and Chilton [1973] and Wallis [1969]). The advantage of this model is that it accounts for inertial forces.

The two-phase flow pressure gradient dP/dx is always greater than the single-phase pressure gradients $(dP/dx)^*_L$ and $(dP/dx)^*_G$ of each phase flowing at the same flow rate. The Lockhart-Martinelli model accounts for this property by introducing two factors, the gas and liquid multipliers Φ_G and Φ_L. For comparison with relative permeabilities, we modified the original definitions by using the gradients of pressure instead of their square roots:

$$\Phi_L = \frac{dP/dx}{(dP/dx)^*_L} \tag{7}$$

$$\Phi_G = \frac{dP/dx}{(dP/dx)^*_G} \tag{8}$$

Instead of the saturation, a new variable χ, the Martinelli parameter, represents the relative importance of the flow of the liquid to the gas flow:

$$\chi = \frac{(dP/dx)^*_L}{(dP/dx)^*_G} \tag{9}$$

These single-phase pressure gradients are calculated by using (4), which takes the inertial forces into account through the experimental h and B values (Figure 3). For the smooth fracture there are no inertial forces and $\chi = \mu_L V_{LS}/ \mu_G V_{GS}$. When (7) and (8) are compared with (5) and (6) for the smooth fracture, it is apparent that $1/\Phi_L$ and $1/\Phi_G$ are analogous to Kr_L and Kr_G. The Lockhart-Martinelli model can be seen as a generalization of Darcy's law for non-Darcy flows.

The plot of $1/\Phi_L$ and $1/\Phi_G$ versus $\chi/(1 + \chi)$, which increases from zero for gas flow to unity for liquid flow, is shown in Figures 7a and 7b. It appears that there is no unique relationship between $1/\Phi$ and χ and that the sum of $1/\Phi_L$ and $1/\Phi_G$ is less than 1. Similar to Figures 6a and 6b, the data for each value of V_{LS} fall on a different curve, although using the Lockhart-Martinelli model makes the data "nearly" collapse onto a single curve, especially for the rough fractures.

Furthermore, the Lockhart-Martinelli model fits the data better when plotted as Φ_G versus χ (Figures 8a and 8b). Curves of the empirical Lockhart and Martinelli relationship
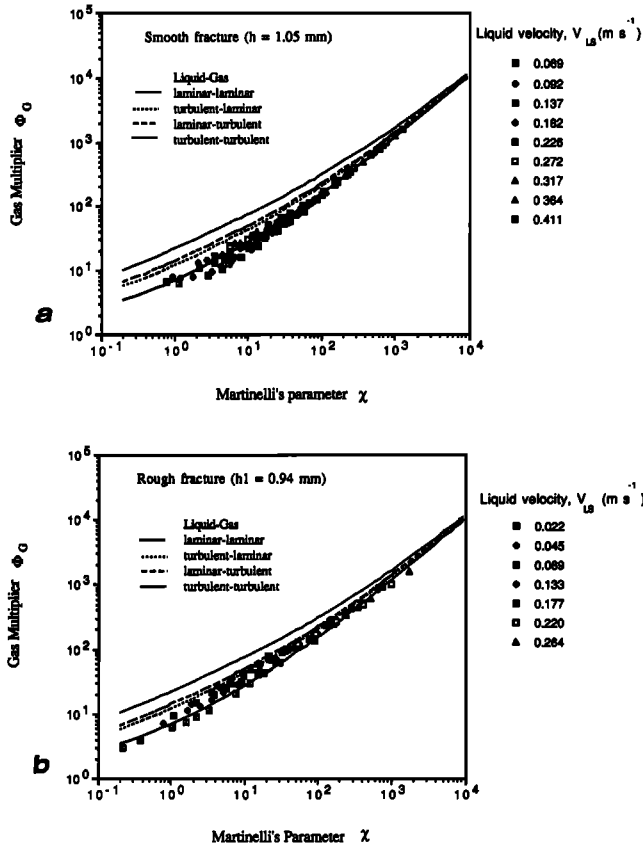
Fig. 8. Data fit to Lockhart-Martinelli model: (a) smooth fracture; (b) rough fracture.

are also plotted in Figures 7a and 7b and Figures 8a and 8b [Delhaye et al., 1981]:

$$\Phi_G = 1 + C\sqrt{X} + X \qquad (10)$$

$$\Phi_L = 1 + \frac{C}{\sqrt{X}} + \frac{1}{X} \qquad (11)$$

where the value of C depends on whether each phase is laminar or turbulent: liquid laminar, gas laminar, $C = 5$; liquid turbulent, gas laminar, $C = 10$; liquid laminar, gas turbulent, $C = 12$; liquid turbulent, gas turbulent, $C = 20$.

Good agreement is obtained with smooth-fracture experimental data and with the Φ_G relationship for laminar-laminar flow ($C = 5$, Figure 8a). This suggests that the Lockhart-Martinelli model might be useful for rough calculations of pressure drop although not for liquid saturation. In discussing Lockhart and Martinelli's original model, *Bergelin and Gazley* [1949] presented two-phase pipe flow data that behave similarly to our data in Figures 7 and 8. This observation suggests that if the Lockhart-Martinelli model can be modified to better fit our fracture flow data, the same modification might also improve the value of the model in predicting pressure drops in pipe flow.

Homogeneous Flow Model

Another empirical approach based on pipe flow models is to treat the two phases like a single homogeneous phase. In this approach, average values for the fluid properties are

defined and the pressure gradient is calculated by using the friction factor, which is empirically related to an average Reynolds number. For two-phase flow in a horizontal pipe [*Delhaye et al.*, 1981]:

$$-\frac{dP}{dx} = \frac{\pi}{A} \tau_w + \frac{d}{dx} [S_L \rho_L V_L^2 + S_G \rho_G V_G^2] \qquad (12)$$

where A and π represent the pipe area and perimeter, τ_w is the average wall shear stress, and V_L and V_G are the local fluid velocities related to superficial velocities by $V_L = V_{LS}/S_L$ and $V_G = V_{GS}/S_G$. The two terms on the right-hand side of (12) can be seen as frictional and accelerational components of the pressure gradient.

The accelerational component of the pressure gradient cannot be calculated, because only average, not local, values are known for S_L (hence for V_L and V_G). However, the accelerational component can be estimated in two limiting cases: (1) S_L (and therefore V_L) remains constant through the fracture, and V_G increases as gas bubbles expand owing to reduced pressure; or (2) V_G remains constant through the fracture so that S_L decreases as gas bubbles expand. The term $(S_L \rho_L V_L^2 + S_G \rho_G V_G^2)$ is evaluated at inlet and outlet, and the difference is compared to the observed pressure drop. This quantity is small under either assumption for all the experiments in the smooth fracture. We therefore disregard the accelerational component and attribute the pressure gradient to friction.

We express the wall shear forces in terms of a friction factor C_f and a mean hydraulic diameter according to the standard definition for single-phase pipe flow. The average wall shear stress is

$$\tau_w = \tfrac{1}{2} C_f \rho_m V^2 \qquad (13)$$

where V is the superficial velocity of the mixture:

$$V = \frac{Q_L + Q_G}{A} \qquad (14)$$

and ρ_m is the mean density:

$$\rho_m = \frac{\rho_L Q_L + \rho_G Q_G}{Q_L + Q_G} \qquad (15)$$

We can also define an average viscosity of the mixture. We use the definition adopted by *Dukler et al.* [1964], which is consistent with our definition of average density:

$$\mu_m = \frac{\mu_L Q_L + \mu_G Q_G}{Q_L + Q_G} \qquad (16)$$

The pressure gradient is obtained by substituting (13) into (12):

$$\frac{dP}{dx} = 2 C_f \rho_m \frac{V^2}{D} \qquad (17)$$

where D is the hydraulic diameter (defined as 4 times the hydraulic radius; in a fracture, $D = 2h$).

We now define Re_2, the two-phase Reynolds number, using the hydraulic diameter of the fracture and the average fluid properties:
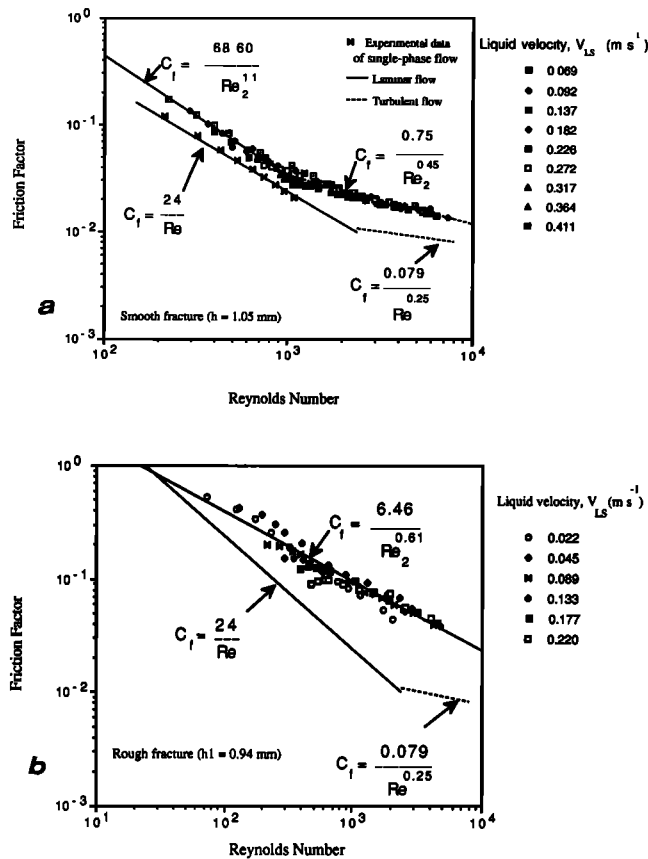
Fig. 9. Friction factor C_f and two-phase Reynolds number Re_2 relationship: (a) smooth fracture; (b) rough fracture.

Fig. 10. Prediction of two-phase pressure gradient by the Lockhart-Martinelli model (10): (a) smooth fracture; (b) rough fracture.

$$Re_2 = \frac{2hV\rho_m}{\mu_m} \qquad (18)$$

With the data from our two-phase flow experiments, we plot C_f against Re_2 for the smooth fracture in Figure 9a and one rough fracture in Figure 9b. The data for single-phase liquid flow and data reviewed by Romm [1966] are also plotted for the smooth fracture. Note that our values of Re are greater than those of Romm by a factor of 4 owing to the definition of the hydraulic diameter.

Several features can be noted for these plots. The correlation is indeed better for the smooth fracture than for the rough fractures. First, we note that the data follow a line with slope equal to -1 at small Re_2, the same as for single-phase flow. The line summarizing Romm's data shows a break in slope to -0.25 above $Re = 2400$; this marks the boundary between laminar and turbulent flows. Our data also show a slope break at $Re_2 = 1000$. However, this change of slope does not correspond to a change of flow regime. For instance, bubble flow appears on either side of the break, and several experiments with different flow regimes have the same average Re_2. Contrary to single-phase flow, the same value of the two-phase Reynolds number does not imply dynamic similarity of the flow.

The coefficient C_f is found to be greater for two-phase flow than for single-phase flow. A rough estimate of the pressure drop can be calculated by using the mean line drawn through the experimental points (in log-log scale, Figures 9a and 9b): For the smooth fracture ($Re_2 < 10^3$),
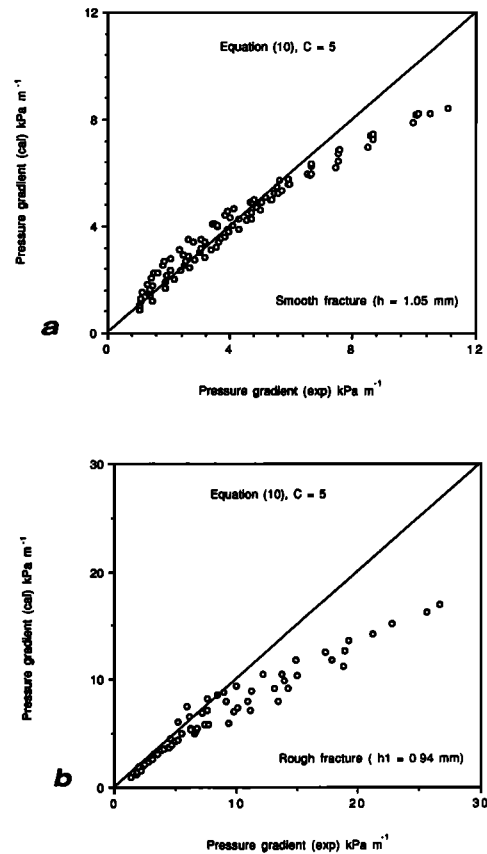
$$C_f = \frac{68.60}{Re_2^{1.1}} \qquad (19)$$

for the smooth fracture ($Re_2 > 10^3$),

$$C_f = \frac{0.75}{Re_2^{0.45}} \qquad (20)$$

for the rough fracture (R1),

$$C_f = \frac{6.46}{Re_2^{0.61}} \qquad (21)$$

Comparison of Models

First, we can discard the relative permeability approach, because it cannot account for inertial forces, which are dominant in our experiments. However, this approach could be useful for flows at smaller Reynolds numbers.

The two other models are predictive. That means that the pressure drop for any liquid and gas flow rate can be calculated by using the experimental law determined in the previous section. In order to compare these two approaches, we have plotted the calculated versus experimental values of pressure drop for the smooth fracture in Figures 10a, 10b, 11a, and 11b. The fit is better with the homogeneous model over the entire range of pressure gradients.

However, we should point out that these two models are able to represent different experiments but always with the
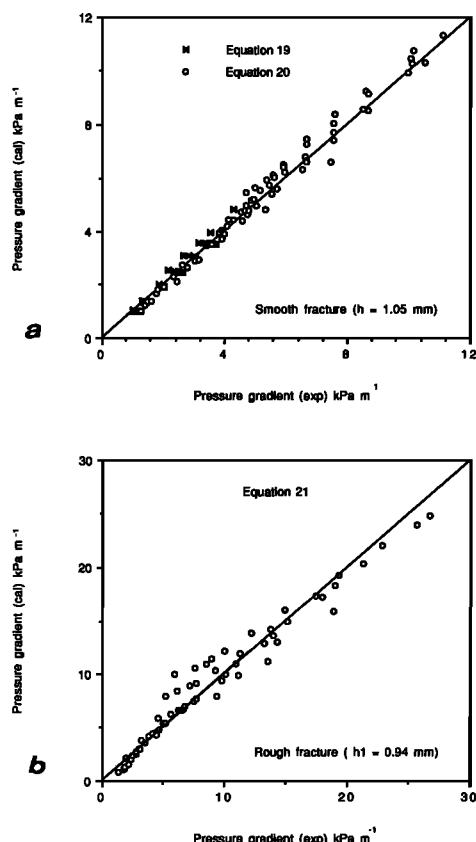
Fig. 11. Prediction of two-phase pressure gradient by the homogeneous model: (a) smooth fracture (equations (19) and (20)); (b) rough fracture (equation (21)).

same fracture. The main question is how to generalize these models so that our empirical results can be used for other fractures.

CONCLUSIONS

Two-phase (air-water) flow experiments were conducted in smooth and artificially roughened fractures with a hydraulic aperture of approximately 1 mm. Gas and liquid superficial velocities ranged from 1.3 to 500 cm s^{-1} and from 0.4 to 40 cm s^{-1}, respectively. Under these conditions, the results of the experiments support the following conclusions.

1. No static flow paths are formed for each phase; instead, moving flow structures in which generally only one phase is continuous are formed. These structures vary with gas and liquid flow rates.

2. Contrary to what is commonly assumed, experimental data show that the relative permeabilities are not linearly dependent on saturation. The data cannot be correlated by using the two-phase Darcy model with relative permeabilities. The data fall on curves showing the same general behavior (phase interference) in both cases; however, different curves result from different liquid velocities.

3. The Lockhart-Martinelli equation leads to a better fit with experiments, at least for the smallest value of the pressure drop.

4. The best fit is obtained by using an empirical homogeneous model in which all the fluid properties are averaged. The pressure drop is then calculated by using a correlation

between the friction factor and the average Reynolds number.

REFERENCES

Bergelin, O. P., and C. Gazley, Co-current gas liquid flow, I, Flow in horizontal tubes, in *Second Heat Transfer and Fluid Mechanics Institute*, pp. 5–18, American Society of Mechanical Engineers, New York, 1949.

Brown, S. R., and R. L. Kraus, Correlation between the surfaces of natural rock joints, *Geophys. Res. Lett.*, *13*, 1430–1433, 1986.

Cox, B. L., and J. S. Y. Wang, Single fracture aperture patterns: Characterization by slit-island fractal analysis, paper presented at International High-Level Waste Management Conference, Am. Nucl. Soc., Las Vegas, Nev., April 26–30, 1993.

Delhaye, J. M., M. Giot, and M. L. Riethmuller, *Thermohydraulics of Two-Phase Systems for Industrial Design and Nuclear Engineering*, pp. 206–207, McGraw-Hill, New York, 1981.

Dukler, A. E., M. Wicks, and R. G. Cleveland, Frictional pressure drop in two-phase flow: Comparison of existing correlation for pressure loss and hold-up, *AIChE J.*, *10*(1), 38–43, 1964.

Fourar, M., Analyse expérimentale et modélisation des écoulements diphasiques en fracture, thèse de doctorat, Inst. Natl. Polytech. de Toulouse, Toulouse, France, 1992.

Fourar, M., J. Piquemal, and S. Bories, Ecoulement diphasique bidimensionel plan liquide-gaz, 2, Gradients de pression et fractions volumiques des phases d'un écoulement horizontal, *C. R. Acad. Sci., Ser. 2*, *313*(2), 477–480, 1991.

Houpeurt, A., *Mécanique des Fluides dans les Milieux Poreux: Critiques et Recherches*, Editions Technip, Paris, 1974.

Lockhart, R. W., and R. C. Martinelli, Proposed correlation of data for isothermal two-phase, two-component flow in pipes, *Chem. Eng. Prog.*, *45*, 39, 1949.

Mendoza, C. A., and E. A. Sudicky, Hierarchical scaling of constitutive relationships controlling multi-phase, paper presented at Third International Reservoir Characterization Technical Conference, Natl. Inst. for Pet. and Energy Res. and U.S. Dep. of Energy, Tulsa, Okla., Nov. 3–5, 1991.

Perry, R. H., and C. H. Chilton, *Chemical Engineers' Handbook*, 5th ed., chap. 5, pp. 5–40, McGraw-Hill, New York, 1973.

Persoff, P., K. Pruess, and L. Myer, Two-phase flow visualization and relative permeability measurement in transparent replicas of rough-walled rock fractures, paper presented at Sixteenth Stanford Geothermal Workshop, Stanford University, Stanford, Calif., Jan. 25–27, 1991.

Pruess, K., and Y. V. Tsang, On two-phase relative permeability and capillarity in rough-walled rock fractures, *Water Resour. Res.*, *26*(9), 1915–1926, 1990.

Pruess, K., G. S. Bodvarsson, and V. Stefansson, Analysis of production data from the Krafla geothermal field, Iceland, paper presented at Ninth Workshop on Geothermal Reservoir Engineering, Stanford University, Stanford, Calif., 1983.

Pruess, K., G. S. Bodvarsson, V. Stefansson, and E. T. Eliasson, The Krafla geothermal field, Iceland, 4, History match and prediction of individual well performance, *Water Resour. Res.*, *20*(11), 1561–1584, 1984.

Pyrak-Nolte, L. J., D. Helgeson, G. M. Haley, and J. W. Morris, Immiscible fluid flow in a fracture, in *Proceedings of the 33rd U.S. Rock Mechanics Symposium*, edited by J. R. Tillerson and W. R. Wawersik, pp. 571–578, Balkema, Rotterdam, Netherlands, 1992.

Raven, K. G., K. S. Novakowski, and P. A. Lapcevic, Interpretation of field tracer tests of a single fracture using a transient solute storage model, *Water Resour. Res.*, *24*(12), 2019–2032, 1988.

Romm, E. S., *Fluid Flow in Fractured Rocks* (in Russian), Nedra Publishing House, Moscow, 1966. (Engl. transl., W. R. Blake, Bartlesville, Okla., 1972.)

Schrauf, T. W., and D. D. Evans, Laboratory studies of gas flow

through a single natural fracture, *Water Resour. Res.*, *22*(9), 1038–1050, 1986.

Temeng, K. O., and R. N. Horne, The effect of high pressure gradients on gas flow, paper SPE-18269 presented at 63rd Annual Technical Conference and Exhibition, Soc. of Pet. Eng., Houston, Tex., 1988.

Wallis, G. B., *One Dimensional Two-Phase Flow*, McGraw-Hill, New York, 1969.

Witherspoon, P. A., J. S. Y. Wang, K. Iwai, and J. E. Gale, Validity of cubic law for fluid flow in a deformable rock fracture, *Water Resour. Res.*, *16*(6), 1016–1024, 1980.

S. Bories and M. Fourar, Institut de Mecanique des Fluides de Toulouse, Avenue du Professeur Camille Soula, 31400 Toulouse, France.

R. Lenormand, Institut Français du Pétrole, BP 311, 92506, Rueil Malmaison, France.

P. Persoff, Earth Sciences Division, Lawrence Berkeley Laboratory, Berkeley, CA 94720.